Nanoscale

Accepted Manuscript

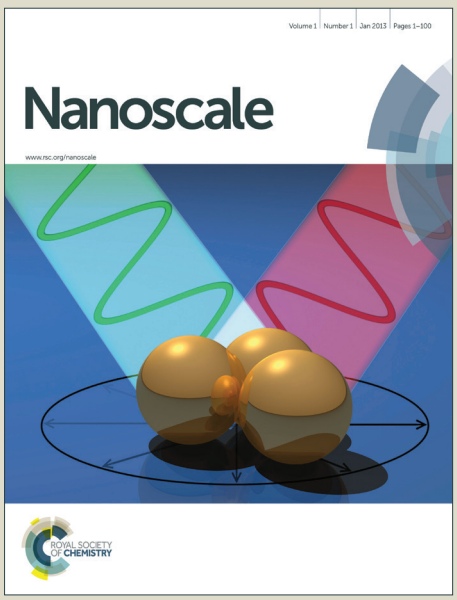

ROYAL SOCIETY OF CHEMISTRY

www.rsc.org/nanoscale

Cite this: DOI: 10.1039/c0xx00000x

www.rsc.org/xxxxxx

ARTICLE TYPE

Improved catalytic activity of Rhodium monolayer modified Nickel (110) Surface for the methane dehydrogenation reaction: A first-principles study

Pallavi Bothra[1] and Swapan K. Pati [1, 2]*

New Chemistry Unit [1] and Theoretical Sciences Unit[2] Jawaharlal Nehru Centre for Advanced Scientific Research, Bangalore, 560064, India.

Received (in XXX, XXX) Xth XXXXXXXXX 20XX, Accepted Xth XXXXXXXXX 20XX

DOI: 10.1039/b000000x

The catalytic activity of pure Ni (110) and single Rh layer deposited Ni (110) surface for the complete dehydrogenation of methane is theoretically investigated by means of gradient-corrected periodic density functional theory. A detailed kinetic study, based on the analysis of the optimal reaction pathway for the transformation of CH_4 to C and H through four elementary steps ($CH_4 \rightarrow CH_3 + H$; $CH_3 \rightarrow CH_2 + H$; $CH_2 \rightarrow CH + H$; $CH \rightarrow C + H$) is presented for pure Ni (110) and Rh/Ni (110) surfaces and compared with pure Rh (110) surface. Through systematic examination of adsorbed geometries and transition states, we show that single layer deposition of Rh on Ni (110) surface has striking influence on lowering the activation energy barrier of the dehydrogenation reaction. Moreover, it is found that, pure Ni (110) surface has tendency of carbon deposition on the catalytic surface during the methane dissociation reaction which decreases the stability of catalyst. However, deposition of carbon is largely suppressed by the addition of Rh overlayer on pure Ni (110) surface. The physical origin of stronger chemisorption of carbon on Ni (110) relative to Rh/Ni (110) has been elucidated by getting insight into the electronic structures and d-band model of the catalytic surfaces. Considering the balance in both the catalytic activity as well as the catalyst stability, we propose that Rh/Ni (110) surface possess much improved catalytic property than pure Ni (110) and pure Rh (110) surfaces.

Introduction

Conversion of methane into high value-added products is like solving two fundamental issues with a single action. Firstly, methane, the second most prevalent and potent greenhouse gas found in the atmosphere, pilots global warming through absorbing radiation within the thermal infrared range. Although methane spans much shorter lifetime in the atmosphere than carbon dioxide, but the former is more effective at trapping radiation and thus is more competent as green house gas. Therefore, reducing the

amount of this gas from the environment has turned out to be one of the paramount challenges; secondly, methane, the most abundant constituent of natural gas, agriculture byproducts possesses high H to C ratio, so can be exploited to fulfill the demand for alternative energy resources. However, the pure tetrahedral methane, with noble-gas like electronic configuration with strong C-H bonds (4.5 eV) and devoid of polarity, magnetic moment and functional group, makes the molecule thermodynamically very stable that it is extremely difficult to undergo any chemical attack. Accordingly, activation of this less reactive, cheap raw material into some clean energy fuels viz. hydrogen has been fuelling the attention of researchers for more than a few decades; [1, 2] however, entire dissociation process is only achievable in the presence of catalyst. [6-8] Single-crystal close-packed surfaces as well as corrugated metal surfaces with low to high indices planes, [9-12] bimetallic alloys, [13-15] metal nanoparticles, [16-19] supported transition metals [20, 21] etc. have been proven as promising catalysts for facilitating the methane dissociation reaction. Amongst all, Ni is found to be the most preferred transition metal catalyst from the both activity as well as cost point of view; [5, 22-25] yet the implementation of Ni for this particular reaction is not widespread due to the tendency of depositing carbon on the catalyst surface and subsequently the growth of filamentous carbon from the segregation and precipitation of C encapsulating the entire catalytic surface, decreasing completely the efficiency of catalysis. [26-29] However, other transition metals, especially, Rh and Ru are being used which exhibit higher catalytic activity as well as stability [2, 8, 30-35] due to higher expenditure and less availability, the application of these metals are limited. Significant theoretical studies have been devoted to comprehend the catalytic process on various Rh surfaces including flat, defect-free, stepped, kinked, nanorod models, to name a few [9-12] and it is generally suggested that on Rh catalyst, methane dissociation is a structure-sensitive reaction.[36-40] Of late, Ni catalyst modified with various transition metals are also in vogue as heterogeneous catalyst because of the synergistic effect exerted by bimetallic catalysts over parent metals.[41-53] Chen *et. al.* thoroughly investigated the effect of substitution of single transition metal atom (Cu, Ru, Rh, Pd, Ag, Pt, Au) on Ni (111) surface and concluded that Rh atom tailored Ni (111) surface is a good candidate for the concerned reaction because of modification in electronic structure.[54] It is moreover reported that foreign atom substitutions can suppress the coke formation on Ni surface by enhancing the Ni metallic dispersion as well as aggregation of Ni nanoparticles during the high temperature reaction.[47, 52]

The main aim of the present work is to study theoretically the kinetics of each elementary step in the sequential dehydrogenation of methane considering CH_3, CH_2 and CH as intermediates, detected in secondary ion mass spectroscopy (SIMS) and X-ray photoelectron spectroscopy (XPS) techniques.[55, 56] The stepwise mechanism has been compared and contrasted among Rh monolayer modified Ni (110) surface, clean Ni (110) and clean Rh (110) surfaces. Top view of all the three surfaces is depicted in Figure 1. The motivation for employing the parent surface as 110 is the kinetic measurements performed by Beebe *et. al.* under high incident flux conditions, [57] which suggested that Ni (110) is the best one amongst Ni (111), Ni (110) and Ni (100) surfaces for methane dissociation reaction but till now no kinetic study has been carried out theoretically. Secondly, single overlayer of Rh has been deposited on Ni (110) surface to detect the role of promoter on catalytic activity and stability over pure Ni (110) surface; recently a number of studies have been shown that overlayers (OLs) or near-surface alloys (NSAs) hold very unusual characteristics compared to their parent surfaces, mostly these bimetallic surfaces show better catalytic activity.[67] By metal deposition method, galvanic displacement, less noble metal monolayer deposited at underpotentials can be substituted by foreign metal monolayer. [68, 69]

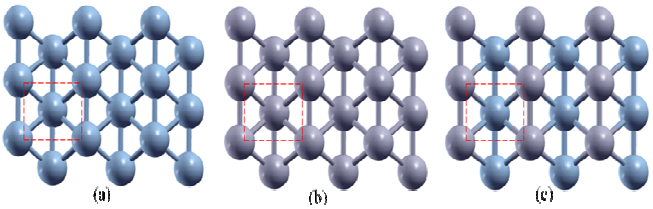

Figure 1. Representation of the top view of three surfaces employed in the present work: (a) Ni (110), (b) Rh (110) and Rh/Ni (110) surface. Ni and Rh atoms are displayed in blue and grey colour, respectively. The red dashed line epresents the unit cell.

Again due to higher price of noble metal, Rh, only one layer of it has been used to cover up the Ni (110) surface. However, pure Rh (110) surface is considered merely for comparison between single and bimetallic surface. After knowing kinetics and mechanism for each step of dissociation reaction, we would do the analysis of electronic structure to understand the physical origin of improved catalytic efficiency of one over other surfaces. Indeed, the

microscopic picture is very much required to design the better catalyst in future.

Computational Details

The quantum-chemical calculations were performed using Quantum Espresso package, [58] in which the wave functions at each k-point are expanded with a plane wave basis set with a kinetic energy cut off up to 400 eV. The approximation, taken into account throughout the density functional theory calculations, was the generalized gradient approximation functional proposed by Perdew, Burke, and Ernzerhof, known as GGA-PBE.[59] Ultrasoft pseudopotentials from the publicly available repository of the QUANTUM ESPRESSO distribution were applied to describe the ionic cores.[60] Brillouin zone sampling was carried out using a Monkhorst-Pack grid for all the calculations and electronic occupations were determined using a Marzari-Vanderbilt scheme with an energy smearing of 0.1 eV.[60] Due to the presence of magnetic element (Ni) in our systems and since accurate quantitative description of the total energies is directly related to surface magnetism, consideration of spin-polarized effects is very essential.[60] Once the difference between the total energy between two consecutive electronic optimization steps were smaller than 10^{-5} eV, the convergence of the electronic degrees of freedom was considered to be attained. The condition for the ionic relaxation was set such that the forces should be less than 10^{-3}eV/Å for all the ions. No symmetry constraints were put in force.

It is already known that the consideration of van-der Waals interaction is necessary for an accurate quantitative description of the total energies; that is why dispersion corrections were taken into account.[61] The Ni (110), Rh (110) and Rh/Ni (110) surfaces were represented as a two-dimensional slab in a 3D periodic cell. The Ni (110) and Rh (110) models employed in this study consist of four-layer slab with a periodic (3×3) unit cell (1/9 monolayer (ML)); then, the Rh/Ni (110) surface was constructed by replacing the uppermost layer of Ni (110) surface by Rh (110). Tests were performed with (2×2) unit cell (1/4 monolayer (ML) coverage) and found that difference in the adsorption energy is the order of 0.13 eV with respect to (3×3) unit cell which suggests the effective lateral interactions between the adsorbate species and their own periodic images from adjacent cells. To check the saturation coverage we did try with (4×3) unit cell (1/12 monolayer (ML)); the difference in energy is in the order of 0.01 eV which indicates the very weak lateral interaction between adsorbates. The computed equilibrium lattice constant for bulk nickel is 3.50 Å, in good agreement with the experimental value (3.52 Å). To circumvent periodic interactions, a vacuum layer of 12Å was used along the perpendicular direction to the surface. The optimized geometries have been achieved by applying analytical calculations of Hellmann-Feynman forces acting on the atoms of the unit cell.

Adsorption energies (ΔE_{ads}) of adsorbates were computed by

$$\Delta E_{ads} = E_{surface+adsorbate} - (E_{surface} + E_{adsorbate})$$

where $E_{surface+adsorbate}$ is the total energy of the relaxed surface with the adsorbate, $E_{surface}$ is the total energy of the bare relaxed surface and $E_{adsorbate}$ is the total energy of an isolated adsorbate. The first two terms were calculated considering the same parameters (k-point sampling, energy cutoff, etc.) mentioned above, the last term was obtained by performing spin-polarized Γ-point calculation of the isolated adsorbate placed in the middle of an empty box of dimension 20Å × 20Å × 20Å. In accordance with this definition, the negative value of adsorption energies implies binding between surfaces and adsorbates.

"Climbing Image Nudged Elastic Band-method (CI-NEB)" method [62] was exploited for determining the transition states of reaction pathways for methane dissociation which is actually the variant of the "nudged elastic band" method[63] and has been proven to be a very efficient technique for finding the minimum energy paths of chemical reactions. Convergence of saddle points and minima were considered to be achieved when the maximum force in each degree of freedom was less than 0.03 eV/Å. The zero-point energy correction was not incorporated. However, though the absolute adsorption energies or activation barriers have not been computed but the cancellation of errors allow us to compare the calculated values among the surfaces considered and therefore the variation in the catalytic activity of Ni (110) and Rh/Ni (110) surfaces can be figured out precisely.

RESULTS AND DISCUSSION

Adsorption energetic and structures of CH_x and H species

Details of the energies of the most stable geometries and positions of CH_X and H on the Ni (110), Rh (110) and Rh/Ni (110) surfaces are given in Table 1. The calculated adsorption energies of Ni (110) and Rh (110) are comparable with the values reported by S. G. Wang *et. al.* [65]and B. Wang *et. al.* [66] respectively. The small discrepancies between the energies is due to the selection of larger unit cell size, that is, p (3×3), in the present work as compared to p (2×2) employed in previous studies. The larger unit cell size results

in a lower surface coverage; consequently, diminish the interaction between the adsorbates. Note that, the initials used in Table 1 for the different surface sites are as follows : short-bridged (SB), long-bridged (LB), top (T), top-down (TD).

Table 1. Adsorption energies, (E_{ads}, eV) and sites of CH_X (x = 0-3) on Ni (110), Rh (110) and Rh/Ni (110) surfaces

Surface	CH3	CH2	CH	C
Ni (110)	-1.98(SB)	-3.80(SB)	-6.87(LB)	-13.78(LB)
Rh (110)	-3.28(SB)	-5.50(LB)	-7.51(LB)	-10.42(LB)
Rh/Ni (110)	-2.12(T)	-4.33(SB)	-6.72(TD)	-7.62(TD)

The preferred adsorption site is given in bracket.

Difference in adsorption properties between Rh/Ni (110) and pure Ni (110) is due to the strain effect which is related to the modification of surface electronic structure by the variation in overlapping of various orbitals; [15] however, among CH_3, CH_2, CH and C intermediates, the first two species adsorbs more strongly to Rh/Ni (110) surface which is in contrast to the results obtained by Fan *et. al.*[53] where single Rh atom addition leads to lowering in adsorption energy of CH_3 and CH_2 fragments than pure Ni (111). This is due to the ligand effect stimulated by the interaction between Rh overlayer and adjacent substrate in the present study. However, the last two intermediates, CH and C, show higher binding potency for pure Ni (110) surface, which confirms the previous findings of the coke formation propensity on Ni surface. Nevertheless, the most negative adsorption energies on Rh (110) surface can be explained in the light of d-band theory proposed by Hammer and Norskov. Increase in the adsorption energy, going from CH_3 to C for all the three systems which is consistent with the earlier reported results is due to the increasing number of free valence electrons upon successively reducing the number of H atoms. In fact, the reason behind striking drop in the binding energy of elementary C on Rh/Ni (110) surface (-7.62 eV) can be understood from the electronic structure of the surfaces and would be discussed in the latter part.

Sequential dehydrogenation of methane on surfaces

Following the study of adsorption behavior i.e. adsorption energies and structures of all the possible intermediates involved in the reaction, we need to find out the plausible minimum energy path (MEP) for the successive dehydrogenation from CH_4 to C. In order to scrutinize the mechanism of CH_4 dissociation, the most stable geometry of CH_X has been chosen as initial state and co-adsorbed CH_{X-1} + H species having the lowest E_{ads} is put as the final configurations in the MEP. Among the three catalytic surfaces, Ni (110), Rh (110) and Rh/Ni (110) considered in the present work, kinetic analysis of CH_4 dehydrogenation on Ni (110) and Rh/Ni (110) surfaces have been investigated in detail and compared with Rh (110) surface. Figure 2. portrays the geometries of the initial, transition and final states of each step. Activation energy barriers for each of the four elementary steps throughout the methane transformation reaction have been tabulated in Table 2. Figure 3. presents the comparison between the energy profiles for the transformation of CH_4 to C and H on the two surfaces, Ni (110) and Rh/Ni (110).

Step1: $CH_4^* \rightarrow CH_3^* + H^*$

Dissociation of methane to methyl and hydrogen is the first step of methane dehydrogenation reaction. The adsorption energy of methane on Ni (110) and Rh/Ni (110) surface are -0.2eV and -0.29 eV, respectively, which indicate the physisorption of saturated tetrahedral methane molecule on the surfaces. To form the product, methane molecule comes closer to the respective surface and accordingly one of the carbon-hydrogen (C-H) bonds gets activated; in the transition state, increase in the C-H bond distance leads to methyl and H fragment which sit together, in slightly tilted fashion, on the single Ni and Rh atom of Ni (110) and Rh/Ni (110) surfaces respectively. The calculated activation energies of this step are 0.89 eV and 0.46 eV for the bare Ni (110) and Rh/Ni (110) surfaces respectively and the reported activation energy on pure Rh (110) by Wang *et. al.* is 0.69 eV. [66]

Step2: $CH_3^* \rightarrow CH_2^* + H^*$

The second step, i.e. the conversion of CH_3 to CH_2 and H takes place with the energy barriers of 0.80 eV on Ni (110) surface, 0.25 eV on Rh/Ni (110) surface and 0.31 eV on Rh (110) surface.[66] For Ni (110) surface bridge positions are the most stable site for both the initial and final intermediates of this step, i.e., CH_3, CH_2 and H. While dissociation of C-H bond in the transition state CH_3 has to shift from one bridge site to adjacent one, leaving one bonded H behind, hence in this case, the relatively heavier group (CH_2) has to voyage a distance from initial state to final one. On the other hand, on Rh/Ni (110) surface, CH_3 sits on the top of single Rh atom whereas CH_2 and H prefer nearby bridge sites; therefore in the transition state CH_3 dissociation occurs on top of the Rh atom itself and budging of CH_2 slightly places it in bridge position. Therefore,

this elementary step is more favorable on Rh/Ni (110) surface over bare Ni (110) surface with lower activation energy barrier.

Step 3: $CH_2^* \rightarrow CH^* + H^*$

On both the surfaces, the dissociation takes place over the bridge site and results in the methylidyne in a hollow site. The computed values imply that cleavage of H from CH_2 is difficult step on Rh/Ni (110) surface with rather high activation energy barrier of 0.73 eV and from the reported result by Wang *et. al.*, it is found that for pure Rh (110) surface this step is the most energetically difficult one with the activation energy of 1.15 eV.[66] But the transformation of CH_2 to CH and H occurs with relatively lower barrier of 0.59 eV for the Ni (110) surface.

Step 4: $CH^* \rightarrow C^* + H^*$

The fourth and final step comprises of the formation of surface C and H upon the dissociation of CH; it needs to overcome the activation energy barriers of 0.48 eV on Ni (110) and 0.57 eV on Rh/Ni (110) surface and that of 0.69 eV on pure Rh (110) surface.[66]

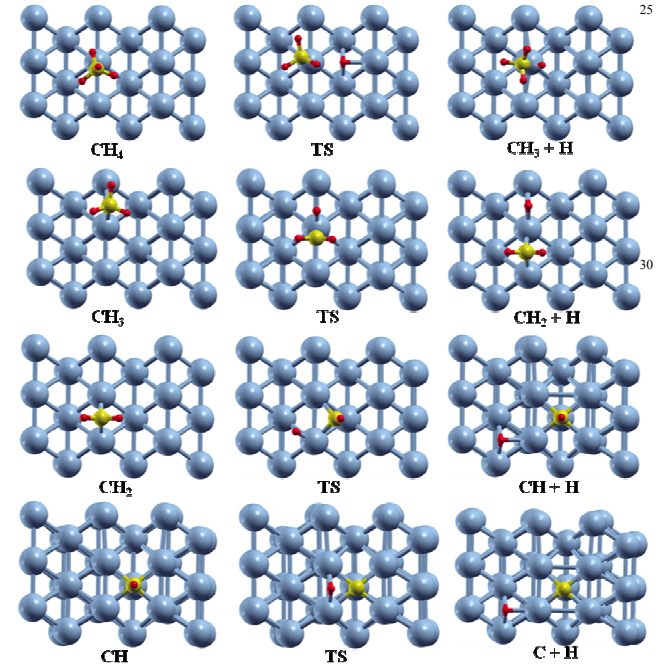

Figure 2 (a). Complete dehydrogenation of CH_4 to C and H on (a) clean Ni (110) surface and with carbon and hydrogen atoms is yellow and red in color respectively. Shown are the optimized initial state, transition state (TS) and final state (from left to right).

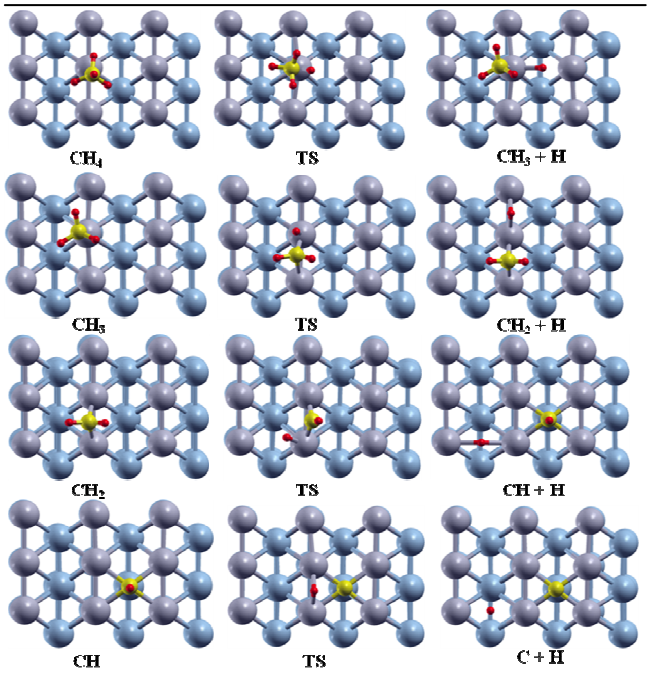

Figure 2 (b). Complete dehydrogenation of CH_4 to C and H on (a) clean Rh/Ni (110) surface and with carbon and hydrogen atoms is yellow and red in color respectively. Shown are the optimized initial state, transition state (TS) and final state (from left to right).

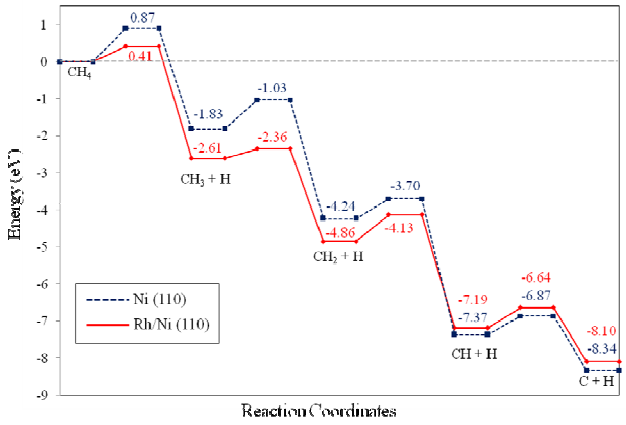

Figure3. Potential energy diagrams for the dehydrogenation of CH_4 on Ni (110) and Rh/Ni (110) surface

Thereby it can be said from Table 2 that the initial two steps ($CH_4 \rightarrow CH_3 + H$; $CH_3 \rightarrow CH_2 + H$) are more feasible on Rh/Ni (110) surface in comparison to Ni (110) surface, however the formation of CH and elementary C ($CH_2 \rightarrow CH + H$; $CH \rightarrow C + H$)

has to overcome a larger barrier of energy 0.73 eV and 0.55 eV for Rh/Ni (110) surface than that of Ni (110) surface with the energy barrier of 0.59 eV and 0.48 eV respectively.

Consequently, from the calculated values, it can be said clearly that carbon formation is less feasible on the Rh layer covered Ni (110) surface than the pure Ni (110) or Rh (110) surface.

Table2. Activation Barriers (eV) for Dehydrogenation of CH_4 to C for various surfaces

	E_{act} (eV)		
Step	Ni (110)	Rh (110) [68]	Rh/Ni (110)
$CH_4 \rightarrow CH_3^* + H^*$	0.89	0.69	0.46
$CH_3^* \rightarrow CH_2^* + H^*$	0.80	0.31	0.25
$CH_2^* \rightarrow CH^* + H^*$	0.59	1.15	0.73
$CH^* \rightarrow C^* + H^*$	0.48	0.69	0.55

Electronic Properties

Till now, the energetics i.e. adsorption and activation energies for the stepwise dehydrogenation reaction of methane to C and 4 H have been computed systematically for bare Ni (110) and Rh monolayer substituted Ni (110) surfaces and it is found that affinity of coke formation is markedly high for clean Ni surface as was found in earlier studies whereas presence of Rh monolayer on Ni (110) surface can diminish the adsorption energy of carbon significantly. The difference in the carbon adsorption energy of Ni (110) and Rh/Ni (110) indicates that there is variation in electronic structure; accordingly, to gain insight of the physical origin, d-band model proposed by Hammer and NØrskov was employed.[70, 71] The average energy of the d-band (also known as d-band centre), ε_d and average width of the d-band, W_d, are imperative parameters to determine the reactivity of various metals involved in reaction. ε_d can be calculated by using the following formula

$$\varepsilon_d = \frac{\int_{-\infty}^{E_F} E\rho_d(E)dE}{\int_{-\infty}^{E_F} \rho_d(E)dE}$$

Likewise, W_d can be obtained according to

$$W_d = \sqrt{\frac{\int_{-\infty}^{E_F} E^2\rho_d(E)dE}{\int_{-\infty}^{E_F} \rho_d(E)dE}}$$

Where, ρ_d is the density of states projected onto metal atom's d-band and E_F represents the Fermi energy.

In general, higher the d-band energy i.e., closer to the Fermi energy level of the d-band center, higher is the reactivity of the corresponding surface metal; alternatively, lower d-band width implies more reactive surface metal atom. This can be understood from the fact that since ε_d shifts up, antibonding states move above the Fermi level. More the number of vacant antibonding states, stronger is the bonding between surface and adsorbate , i.e., strong chemisorption. Table 3 lists the values of ε_d and W_d for carbon containing Ni (110) and Rh/Ni (110) surfaces. Higher average energy as well as lower band width of carbon containing Ni (110) compared to Rh/Ni (110) explains the more negative adsorption energy i.e., stronger adsorption of carbon on the former surface than the latter one.

Table 3. Average Energy (ε_d) and Width (W_d) of the d-band of C adsorbed surface atoms

Surface	Surface + C[a]	
	ε_d (eV)	W_d (eV)
Ni (110)	-1.53	1.37
Rh/Ni (110)	-1.75	2.42

[a]Atoms involved in C adsorption are considered

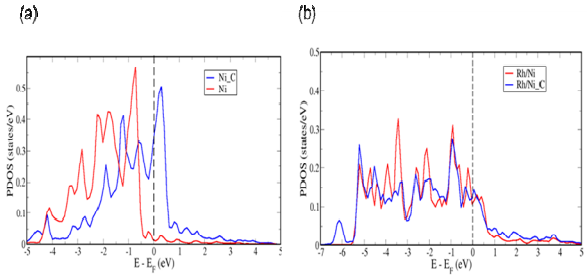

Figure 4. Projected Density of States for (a) Pure Ni (110) surface and surface Ni atoms involved in C adsorption and (b) pure Rh/Ni (110) and surface Rh atoms involved in C adsorption. The vertical dotted lines denote the Fermi level.

For completeness, projected density of states (pDOS) analysis of the surface atoms in the presence and absence of elementary carbon on pure Ni (110) and Rh/Ni (110) surfaces has been included in Figure 4 (a) and 4 (b) respectively. Actually, the differences between average energy and d-band width arise due to the difference in interaction between metal d-band and C p-orbitals. In both the cases, for pure Ni (110) and Rh/Ni (110) surfaces,

particularly $d_{x^2-y^2}$ band exhibits a considerable modification after the adsorption of carbon in the Fermi level, whereas the main features of the other bands are less prominent. From the comparison of carbon containing Ni (110) and Rh/Ni (110) surfaces, it is found that antibonding orbitals are more shifted above the Fermi level for Ni (110) surface than the latter, i.e., weight of the energy contributions above the Fermi level is larger in Ni (110) surface. Subsequently, the Ni-C antibonding levels are mostly emptied on Ni (110) surface than on the Rh/Ni (110) surface. Consequently, this behavior confirms the stronger adsorption of carbon on clean Ni (110) surface.

Conclusions

We have computed the energetics as well as kinetics of entire dehydrogenation of CH_4 to C and H on Ni (110) and Rh/Ni (110) surfaces. For Ni (110) surface, the first dissociation step ($CH_4 \rightarrow CH_3 + H$) is rate controlling with activation energy barrier 0.89 eV while for Rh/Ni (110), the third dissociation step ($CH_2 \rightarrow CH + H$) determines the rate of the reaction and it requires 0.73 eV amount of energy to overcome the barrier. However, on Rh/Ni (110) surface, the first two dehydrogenation steps require only 0.46 eV and 0.25 eV amounts of energies to dissociate carbon-hydrogen bond from methane and methyl, respectively. So, the activation of carbon-hydrogen bond for the two consecutive steps, ($CH_4 \rightarrow CH_3 + H$) and ($CH_3 \rightarrow CH_2 + H$) are very facile on Rh covered Ni (110) surface and the resulting hydrogen and carbon-containing species would then serve as building blocks for the production of chemicals and fuels e.g., ethylene or higher alkanes etc.

From the comparison among pure Ni (110), pure Rh (110), and Rh/Ni (110) surfaces, it is found that Rh/Ni (110) surface is the most efficient one in both the activity as well as stability point of view, because, Rh overlayer on Ni (110) surface reduces both the activation energy barriers and the coke formation tendency efficiently in comparison to the pure Ni (110) and pure Rh (110) surfaces; In addition, the physical origin of weaker carbon adsorption affinity of Rh/Ni (110) surface with respect to pure Ni (110) surface has been elucidated from electronic structure analysis.

In summary, our research provides a novel idea to design highly efficient and economically benign bimetallic catalyst for methane dissociation reaction by depositing a single layer of foreign metal on clean surface and the hybrid organization altogether can perform as a very good catalyst for the concerned process with respect to the single crystal surface. Furthermore, the catalytic properties can be tailored largely by introducing bimetallic overlayer on parent metal surface by tuning the electronic plus structural behaviors of the entire system.

AUTHOR INFORMATION

Corresponding Author

Prof. Swapan K Pati, Theoretical Sciences Unit, Jawaharlal Nehru Centre for Advanced Scientific Research, Bangalore, 560064, India..E-mail:pati@jncasr.ac.in

ACKNOWLEDGMENT

PB acknowledges the CSIR for a research fellowship. SKP acknowledges research support from the CSIR and DST, Government of India. We thank Mr. Mohnish Pandey from the department of Physics, Technical University of Denmark for scientific help.

References

1. S. Saadi, B. Hinnemann, S. Helveg, C. C. Appel, F. Abild-Pedersen, and J. K. NØrskov, *Surf. Sci.* **603**, 762 (2009).

2. G. Jones, J. G. Jakobsen, S. S. Shim, J. Kleis, M. P. Andersson, J. Rossmeisl, F. Abild-Pedersen, T. Bligaard, S. Helveg, B. Hinnemann, J. R. Rostrup-Nielsen, I. Chorkendorff, J. Sehested, and J. K. Nørskov, *J. Catal.* **259**, 147 (2008).

3. Irion, W. W.; Neuwirth, O. S. Oil Refining; Wiley: Weinheim, Germany, 2005; pp 152.

4. Topsøe, H.; Clausen, B. S.; Massoth, F. E. Hydrotreating Catalysis, Science and Technology; Springer: Berlin, Germany, 1996.

5. Rostrup-Nielsen, J. R. Steam Reforming Catalysts; Danish Technical Press: Copenhagen, Denmark, 1975; pp 17-37.

6. Paul, JF; Sautet, P, *J. Phys. Chem. B* **102,** 1578 (1998).

7. Lodriguito M.D. , Lendvay G. , and Schatz G. C. , *J. Chem. Phys.* **131**, 224320 (2009).

8. Au, C.-T.; Ng, C.-F.; Liao, M.-S. , *J. Catal.* **185**, 12 (1999).

9. Abild-Pedersen, F.; Lytken, O.; Engbæk, J.; Nielsen, G.; Chorkendorff, I.; Nørskov, J. K. , *Surf. Sci.* **590**, 127 (2005).

10. Honkala, K.; Hellman, A.; Remediakis, I. N.; Logadottir, A.; Carlsson, A.; Dahl, S.; Christensen, C. H.; Nørskov, J. K. , *Science* **307**, 555 (2005).

11. Liu, Z.-P.; Hu, P., *J. Am. Chem. Soc.* **125**, 1958 (2003).

12. P. W. van Grootel; R. A. van Santen, and E. J. M. Hensen *J. Phys. Chem. C* **115**, 13027 (2011)

13. J. W. A. Sachtler and G. A. Somorjai, *J. Catal.* **81**, 77 (1983).

14. P. Liu and J. K. Nørskov, *Phys. Chem. Chem. Phys.* **3**, 3814 (2001).

15. M. Mavrikakis; B. Hammer; and J. K. Nørskov, *Phys. Rev. Lett*. **81**, 2819 (1998).

16. Cheng, Z; Fine, NA ; Lo, CS **55**, 345 (2012).

17. Gonzalez, I. ; D. J. , JC; Canizales, E. ; Delgado B. ; Urbina C. *J. Phys. Chem. C* **116**, 21577 (2012)

18. Vines, F. ; Lykhach, Y.; Staudt, T. ; Lorenz, M. P. A. ; Papp, C. ; Steinruck, H. P. ; Libuda, J. ; Neyman, K. M. ; Gorling, A. *Chem. Eur. J.* **16**, 6530 (2010)

19. Harding, D. J. ; Kerpal, C. ; Meijer, G. ; Fielicke, A. , *Angew. Chem., Int. Ed.* **51**, 817 (2012).

20. Ligthart, D. A. J. M.; van Santen, R. A.; Hensen, E. J. M. , *J. Catal* **280**, 206 (2011).

21. Shen, WQ; Huggins, F. E.; Shah, N; Jacobs, G.; Wang, YG; Shi, XB; Huffman, GP, *Appl. Catal. A* **351**, 102 (2008).

22. Wang, S.-G.; Cao, D.-B.; Li, Y.-W.; Wang, J.; Jiao, H., *J. Phys.Chem. B* **110**, 9976 (2006).

23. Wang, S.-G.; Cao, D.-B.; Li, Y.-W.; Wang, J.; Jiao, H. *Surf. Sci* **600**, 3226 (2006).

24. Watwe, R. M.; Bengaard, H. S.; Rostrup-Nielsen, J. R.; Dumesic,J. A.; Nørskov, J. K. *J. Catal.* **189,** 16 (2000).

25. Sehested, *J. Catal. Today* **111**, 104 (2006).

26. S. Helveg, C. Lopez-Cartes, J. Sehested, P. L. Hansen, B. S. Clausen, J. R. Rostrup-Nielsen, F. Abild-Pedersen, and J. K. Nørskov, *Nature* (London) **427**, 426 (2004).

27. F. Abild-Pedersen, J. K. Nørskov, J. R. Rostrup-Nielsen, J. Sehested, and S. Helveg, *Phys. Rev. B* **73**, 115419 (2006).

28. C. Fan, X. G. Zhou, D. Chen, H. Y. Cheng, and Y. A. Zhu, *J. Chem. Phys.* **134**, 134704 (2011).

29. W. Snoeck, G. F. Froment, and M. Fowles, *J. Catal.* **169**, 250 (1997).

30. Rostrup-Nielsen, J. R.; Bak Hansen, J. H., *J. Catal.* **144**, 40 (1993).

31. Qin, D.; Lapszewicz, *J. Catal. Today* **21,** 552 (1994).

32. Ciobica, I. M.; van Santen, R. A., *J. Phys. Chem. B* **106**, 6200 (2002).

33. Ciobica, I. M.; Frechard, F.; van Santen, R. A.; Kleyn, A. W.; Hafner, J. P. J., *J. Phys. Chem. B* **104**, 3364 (2000).

34. Kokalj, A; Bonini, N.; Sbraccia, C.; de Gironcoli, S.; Baroni, S., *J. Am. Chem. Soc.***126**, 16732 (2004).

35. Bunnik, B. S.; Kramer, G. J. *J. Catal.* **242**, 309 (2006).

36. Wei, J. M.; Iglesia, E., *J. Phys. Chem. B* **108**, 4094 (2004).

37. Wei, J. M.; Iglesia, E., *Angew. Chem., Int. Ed.***43**, 3685 (2004).

38. Wei, J. M.; Iglesia, E. *J. Phys. Chem. B* **108**, 7253 (2004).

39. Wei, J. M.; Iglesia, E. *J. Catal.* **225**, 116 (2004).

40. Wei, J. M.; Iglesia, E. *Phys. Chem. Chem. Phys*. **6**, 3754 (2004).

41. W. An, X. C. Zeng, and C. H. Turner, *J. Chem. Phys.***131**, 174702 (2009).

42. J. H. Lee, E. G. Lee, O. S. Joo, and K. D. Jung, *Appl. Catal., A* **269**, 1 (2004).

43. J. H. Jeong, J. W. Lee, D. J. Seo, Y. Seo, W. L. Yoon, D. K. Lee, and D. H.Kim, *Appl. Catal., A* **302**, 151 (2006).

44. C. Crisafulli, S. Scire, S. Minico, and L. Solarino, *Appl. Catal., A* **225**, 1 (2002).

45. D. L. Li, T. Shishido, Y. Oumi, T. Sano, and K. Takehira, *Appl. Catal., A* **332**, 98 (2007).

46. H. Arbag, S. Yasyerli, N. Yasyerli, and G. Dogu, *Int. J. Hydrogen Energy* **35**, 2296 (2010).

47. S. Takenaka, Y. Shigeta, E. Tanabe, and K. Otsuka, *J. Phys. Chem. B* **108**, 7656 (2004).

48. B. Steinhauer, M. R. Kasireddy, J. Radnik, and A. Martin, *Appl. Catal., A* **366**, 333 (2009).

49. N. V. Parizotto, K. O. Rocha, S. Damyanova, F. B. Passos, D. Zanchet, C.M. P. Marques, and J. M. C. Bueno, *Appl. Catal., A* **330**, 12 (2007).

50. M. Garcia-Dieguez, I. S. Pieta, M. C. Herrera, M. A. Larrubia, and L. J. Alemany, *J. Catal.* **270**, 136 (2010).

51. M. Garcia-Dieguez, I. S. Pieta, M. C. Herrera, M. A. Larrubia, and L. J. Alemany, *Appl. Catal., A* **377**, 191 (2010).

52. A. M. Molenbroek, J. K. Nørskov, and B. S. Clausen, *J. Phys. Chem. B* **105**, 5450 (2001)

53. C. Fan, Y. A. Zhu, Y. Xu, Y. Zhou, X. G. Zhou, and D. Chen *J. Chem. Phys.* **137**, 014703 (2012).

54. M. P. Kaminsky, N. Winograd, G. L. Geofroy, M. Albert Vannice, *J. Am. Chem. Soc.* **108**, 1315 (1986).

55. Q. Y. Yang, K. J. Maynard, A. D. Johnson, S. T. Ceyer, *J. Chem. Phys.* **102**, 7734 (1995).

56. Beebe, T. P., Jr.; Goodman, D. W.; Kay, B. D.; Yates, J. T., Jr., J. Chem. Phys. **87**, 2305.

57. http://www.pwscf.org and http://www.quantum-espresso.org.

58. J. P. Perdew, K. Burke, and M. Ernzerhof, *Phys. Rev. Lett.* **77**, 3865 (1996);

59. Ultrasoft pseudopotentials from the publicly available QUANTUM ESPRESSO table are used: Ni.pbe-nd-rrkjus.UPF, Rh.pbe-nd-rrkjus.UPF, C.pbe-rrkjus.UPF and H.pbe-rrkjus.UPF for GGA calculation.

60. N. Marzari, D. Vanderbilt, and M. C. Payne, *Phys. Rev. Lett.* **79**, 1337 (1997).

61. R. O. Jones and O. Gunnarson, *Rev. Mod. Phys*. **61**, 689 (1989).

62. G. Henkelman, B. P. Uberuaga, and H. Jónsson, *J. Chem. Phys.* **113**, 9901 (2000); **113**, 9978 (2000).

63. H. Jónsson, G. Mills, and K. W. Jacobsen, in *Classical and Quantum Dynamics in Condensed Phase Simulations*, edited by B. J. Berne, G. Ciccotti, and D. F. Coker (World Scientific, Singapore, 1998).

64. Lynch, B. J.; Fast, P. L.; Harris, M. and Truhlar, D. G., J. Phys. Chem.**104**, 4811 (2000).

65. S. G. Wang, D. B. Cao, Y. W. Li, J. Wang and H. Jiao, *Surf. Sci.* **600**, 3226 (2006).

66. B. Wang, L. Song and R. Zhang, *Appl. Surf. Sci.* **258**, 3714 (2012).

67. A. S. Bandarenka, A. S. Varela, M. Karamad, F. C. Vallejo, L. Bech, F. J. P. Alonso, J. Rossmeisl, I. E. L. Stephens, and I. Chorkendorf Angew. Chem. Int. Ed. **51**, 11841 (2012)

68. Brankovic, S. R.; Wang, J. X.; Adzic, R. R., *Surf. Sci.* **474,** L173 (2001).

69. J. Zhang*, M. B.* Vukmirovic*,* Y. Xu*,* M. Mavrikakis*, and* R. R. Adzic*, Angew. Chem., Int. Ed*. **44**, 2132 (2005).

70. B. Hammer and J. K. Nørskov, *Surf. Sci.* **343**, 211 (1995).

71. B. Hammer, O. H. Nielsen, and J. K. Nørskov, *Catal. Lett.* **46**, 31 (1997)

SYNOPSIS TOC